Integrated sustainable aviation fuel (SAF) production routes with enhanced biogenic CO2 utilization through power-to-liquid systems

Vibhu Baibhav[a]*, Daniel Florez-Orrego[a], Meire Ellen Ribeiro Domingos[a], Francois Maréchal[a]

[a] *Industrial Process and Energy Systems Engineering Laboratory, École Polytechnique Fédérale de Lausanne (EPFL), Valais-Wallis, Sion, Switzerland.*
* *vibhu.baibhav@epfl.ch*

Abstract:

The aviation sector is among the most challenging industries to decarbonize, with sustainable aviation fuels (SAF) representing the most viable near-term solution for reducing its carbon footprint. Corn-to-ethanol biorefineries generate concentrated biogenic CO_2 streams during fermentation in near-equimolar proportions to ethanol, which are typically vented to the atmosphere despite representing a significant underutilized carbon resource. This study investigates the integration of these biogenic CO_2 streams into a Power-to-Liquid (PtL) system coupled with an ethanol-to-jet fuel upgrading process, with the objective of improving carbon utilization efficiency and increasing SAF yield.

Two CO_2-to-ethanol conversion pathways are evaluated: (i) catalytic hydrogenation using renewable hydrogen produced via alkaline electrolysis, and (ii) co-electrolysis of CO_2 and H_2O to syngas followed by microbial fermentation. Process models developed in Aspen Plus are used to characterize the mass, energy, and heat integration potential of each pathway. A mixed-integer linear programming (MILP) framework incorporating clustered renewable generation profiles, hourly electricity price dynamics, and a liquefaction-based CO_2 seasonal storage system is developed to optimize the sizing and operation of the integrated system under variable renewable energy conditions.

The heat integration analysis reveals strong thermal complementarity between the ethanol production and jet fuel upgrading processes. The catalytic hydrogenation pathway is identified as the thermally favourable route, exhibiting a net heat-exporting character that enables the integrated system to achieve complete thermal self-sufficiency with no external hot utility requirement. Seasonal CO_2 storage plays a key role in decoupling continuous CO_2 generation from variable renewable electricity availability, enabling near-complete annual utilization of biogenic CO_2. Overall, the integrated system significantly improves carbon utilization efficiency, increases SAF production, and enhances economic performance under variable electricity price conditions. The proposed framework provides a promising pathway for advancing resource-efficient and low-carbon aviation fuel production.

Keywords :
Sustainable aviation fuel (SAF); CO_2 utilization; Power-to-liquid (PtL); Process integration; MILP optimization

1. Introduction

Carbon dioxide (CO_2) emissions continue to rise globally, largely driven by the ongoing reliance on fossil fuels in the energy, transport, and industrial sectors. Transitioning to low-carbon energy systems therefore requires a significant increase in renewable electricity generation, particularly from wind and solar. However, the variable nature of these resources leads to fluctuations in electricity supply, resulting in periods of surplus generation as well as shortages. Addressing this variability is a key challenge in the integration of renewable energy systems.

Several energy storage technologies are available to address short-term fluctuations in electricity supply. Batteries are widely used for fast response and intra-day storage, offering high efficiency and flexibility. Pumped hydro storage is also well established and can provide large-scale storage over daily to weekly timescales. However, both technologies face limitations when it comes to long-term or seasonal storage. Batteries become expensive for large storage capacities and long durations, while pumped hydro is geographically constrained and requires suitable topography and large infrastructure investments.

In addition, these storage options primarily return electricity to the grid and do not directly address the energy needs of other sectors such as transport and industry. In contrast, Power-to-X (PtX) technologies offer a way to convert excess renewable electricity into chemical energy carriers such as hydrogen or synthetic fuels. This enables not only long-term and seasonal energy storage, but also sector coupling by providing low-carbon fuels for applications where direct electrification is difficult.

In particular, Power-to-Liquid (PtL) pathways allow the production of synthetic liquid fuels that can be used within existing infrastructure. This is especially important for the aviation sector, where electrification is not feasible. While alternative solutions such as hydrogen-based aviation are being actively investigated, they would require significant changes to aircraft design, fuel distribution systems, and airport infrastructure. Considering the long lifetime of existing aircraft fleets, sustainable aviation fuels (SAF) are therefore considered the most promising decarbonization option in the near to medium term, as they can be integrated into current systems with minimal modifications.

A key challenge in the deployment of PtL systems is the availability, purity, and cost of CO_2 feedstock. Conventional CO_2 capture technologies, including post-combustion capture from flue gases and direct air capture, are associated with significant energy penalties and high costs, which negatively impact overall system efficiency and economics. In contrast, several biogenic CO_2 sources offer attractive alternatives, including waste-to-energy plants, biogas upgrading processes, biomass-fired power plants, as well as industrial sectors such as cement and pulp and paper production. Among these, bioethanol production is particularly noteworthy. During fermentation, CO_2 is generated in nearly equimolar proportions to ethanol and at high purity levels (typically >99%), making it readily available for utilization with minimal additional processing requirements [1]. Despite these advantages, such concentrated biogenic CO_2 streams are often vented to the atmosphere, representing a significant underutilized carbon resource.

The effective integration of biogenic CO_2 into PtL systems requires accounting for the temporal variability of renewable electricity and its impact on process operation. In this work, hourly data for Switzerland, including ambient temperature, solar irradiation, wind speed, and electricity price, are processed using k-means clustering to derive representative operating conditions. This data-driven approach reduces computational complexity while preserving the key temporal characteristics necessary for system-level optimization. In addition, to address seasonal mismatches between CO_2 supply and renewable electricity availability, the integration of CO_2 storage via liquefaction is considered. This enables the buffering of CO_2 across time, allowing excess CO_2 to be stored during periods of low utilization and subsequently converted during periods of high renewable energy availability, thereby enhancing system flexibility and overall carbon utilization.

While previous studies have investigated PtX systems under dynamic operation, most have focused on hydrogen or methanol production [2], and have not explicitly addressed the integration of high-purity biogenic CO_2 streams within PtL pathways targeting aviation fuels. Furthermore, there remains a lack of studies that combine detailed process modelling with techno-economic optimization under realistic electricity price signals, renewable generation profiles, and emissions constraints, while also considering the role of seasonal storage and operational flexibility.

In this study, an integrated biorefinery–PtL system is investigated, in which CO_2 generated from corn-to-ethanol production is utilized for additional fuel synthesis. Two pathways for converting CO_2 to ethanol are evaluated: (i) catalytic hydrogenation using renewable hydrogen produced via alkaline electrolysis, and (ii) co-electrolysis of CO_2 to syngas followed by fermentation to ethanol. The resulting ethanol is subsequently upgraded to SAF, enhancing the overall carbon utilization efficiency of the biorefinery while contributing to low-carbon aviation fuel production. Process models developed in Aspen Plus are coupled with a system-level optimization framework incorporating clustered renewable generation profiles, electricity price dynamics, and Scope 2 emissions. The objective is to identify optimal design and operational strategies and to quantify improvements in carbon utilization, energy efficiency, and economic performance under variable and seasonal renewable energy conditions.

2. Methodology

The methodology of this study combines detailed process modelling, renewable energy modelling, and system-level optimization to evaluate an integrated biorefinery–Power-to-Liquid (PtL) system for sustainable aviation fuel (SAF) production using biogenic CO_2. The framework integrates process simulation in Aspen Plus with data-driven renewable energy representation and a mixed-integer linear programming (MILP) optimization approach.

2.1. Process modelling

The core biorefinery and fuel synthesis pathways are developed in Aspen Plus using established reference models from the National Renewable Energy Laboratory (NREL). In particular, the corn-to-ethanol production process is based on the model reported in [3], while the ethanol-to-sustainable aviation fuel (SAF) upgrading pathway follows the methodology described in [4]. Both models were adapted to ensure consistency in system boundaries, thermodynamic assumptions, and stream integration within the overall framework. The block flow diagram of the integrated system is shown in Figure 1.

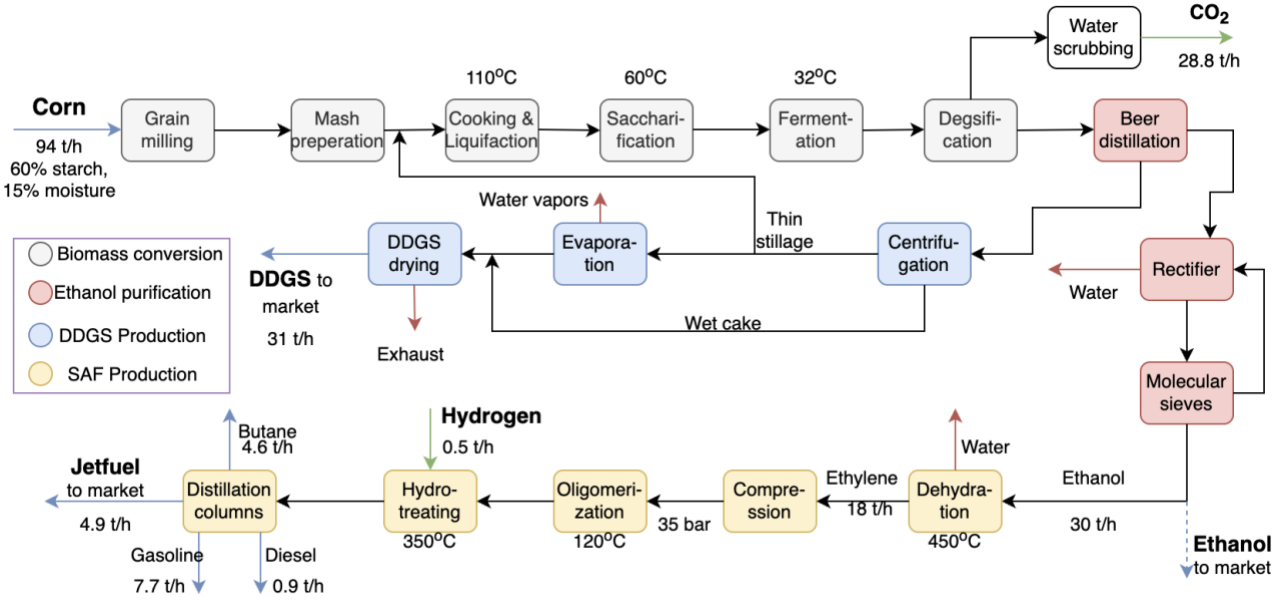

Figure. 1. Simplified process flow diagram of the integrated corn-to-ethanol and ethanol-to-jet fuel production processes, based on Aspen Plus simulations. The diagram highlights major process units along with key mass flow rates and temperatures. DDGS and CO_2 are generated as by-products of ethanol production, whereas gasoline, diesel, and butane are produced as co-products in the jet fuel upgrading section.

In addition, two CO_2-to-ethanol conversion pathways are implemented based on published literature models:

- Catalytic hydrogenation of CO_2 to ethanol, using renewable hydrogen produced via alkaline electrolysis.
- CO_2-to-syngas conversion followed by fermentation, based on co-electrolysis of CO_2 and water.

A schematic representation of both pathways is provided in Figure 2. The modeling approach for each pathway is described separately. Catalytic hydrogenation involves the conversion of CO_2 with renewable hydrogen to ethanol in the presence of a heterogeneous catalyst. Catalysts play a critical role in CO_2 hydrogenation to ethanol, as multiple parallel reactions can lead to the formation of by-products such as methanol and acetic acid [5]. Recent developments have demonstrated selective ethanol production with a space–time yield (STY) of up to 8.65 mmol g_{cat}^{-1} h^{-1} [6].

An Aspen Plus model was developed based on data reported in [7, 8]. A single-pass conversion of 20% was assumed in accordance with [7]. The conversion of CO to ethanol was assumed to be equal to that of CO_2 to ethanol, while the CO_2 conversion via the reverse water–gas shift (RWGS) reaction was taken as one-third of the CO_2-to-ethanol conversion.

The reactor pressure was fixed at 30 bar, based on the sensitivity analysis reported in [8]. Although lower temperatures thermodynamically favor ethanol formation, they result in reduced reaction rates; therefore, a compromise temperature of 200 °C was selected. Due to the low single-pass conversion, unreacted gases were recycled to enhance overall ethanol yield. The recycle split ratio was optimized to 0.95 following the methodology described in [7].

As illustrated in Figure 2, the second pathway consists of the co-electrolysis of CO_2 and H_2O to produce syngas, followed by microbial fermentation to ethanol. Ethanol production via syngas fermentation has been extensively studied in the literature and has also been commercially implemented by LanzaTech [9].

The syngas fermentation process was modeled in Aspen Plus based on data reported in [10], which describes biomass gasification followed by biochemical conversion to ethanol. Clostridium ljungdahlii was selected as the biocatalyst. The process is represented using two fermentation stages: an initial reactor for acidogenesis, where microbial growth occurs, followed by a bubble column reactor for solventogenesis. During acidogenesis, C. ljungdahlii primarily produces acetic acid, whereas in the solventogenic stage, ethanol becomes the dominant product [10]. This shift is driven by the conversion of acetic acid to ethanol via reductive pathways, leading to increased ethanol selectivity.

The biochemical reactions, corresponding fractional conversions, and modeling assumptions, including gas recycling and the omission of nutrient balances, were adopted directly from the reference model [10].

The model was further adapted to reflect the upstream co-electrolysis of CO_2 and H_2O, which provides a syngas stream with the required H_2/CO ratio. The influence of syngas composition on fermentation performance has been investigated in [11], considering different molar ratios of H_2, CO_2, and CO. In this study, the required syngas composition is achieved directly via co-electrolysis, eliminating the need for external hydrogen addition to the second fermentation reactor, as implemented in the reference case.

Electricity price is a key driver of the overall process economics. A study by the National Renewable Energy Laboratory (NREL), USA, reports that bioelectrochemical conversion pathways for CO_2-to-ethanol can achieve significant cost reductions under low electricity price scenarios [12]. This aspect is therefore explicitly considered in the economic evaluation of the process.

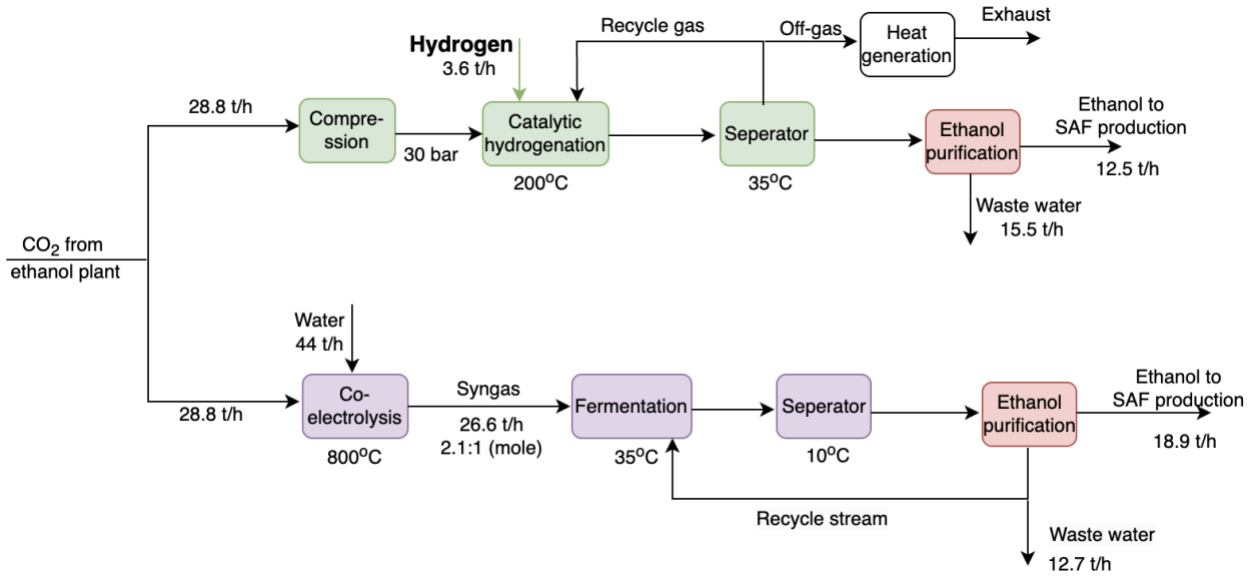

Figure. 2. Block flow diagram of CO_2 utilization pathways for ethanol production: (a) catalytic hydrogenation using renewable hydrogen, and (b) co-electrolysis to syngas followed by fermentation. Both pathways include an ethanol purification section, consisting of distillation columns, as shown in Figure 1.

2.2. Renewable energy integration and data processing

For the catalytic hydrogenation pathway, electrochemical hydrogen production is modelled using alkaline electrolysis. A CO_2 storage system based on liquefaction is also included to enable temporal decoupling between CO_2 availability and utilisation. The electrolyser model, along with the CO_2 storage system, is explained in [13], whereas the co-electrolysis model for syngas fermentation is adapted from [14]. Since electricity and hydrogen are major contributors to both the economic cost and life cycle environmental impacts of CO_2 utilisation pathways, the source and supply conditions of these energy carriers are central to the assessment framework. Integrating renewable electricity generation directly into the optimisation, therefore, allows the model to capture the full cost and emission implications of local renewable supply versus grid electricity procurement.

To represent the variability of renewable energy supply, hourly data for Switzerland are used, including solar irradiation, wind speed, ambient temperature, and electricity price. These data, sourced from [15], are processed using K-means clustering to generate a reduced set of representative typical days, preserving key temporal patterns in renewable resource availability and electricity price dynamics while maintaining computational tractability.

Photovoltaic and wind turbine models are used to estimate renewable electricity generation based on the clustered meteorological data. The mathematical formulations and parameter values for both models are taken from [16] and [17] and explained in Appendix A. The resulting electricity supply profiles are then coupled with the process models through their respective electricity and heat demands.

The K-means algorithm is applied to the complete 8,760-hour annual dataset, with each day described by its 24-hour profiles of four input parameters: electricity price (€/MWh), external ambient temperature T_{ext} (°C), global solar irradiance GI (W/m²), and wind speed V_{wind} (m/s). Each day is therefore represented as a feature vector of 96 values (4 parameters × 24 hours), and the algorithm partitions the 365 days of the year into K = 10 clusters by minimising the within-cluster sum of squared distances. The occurrence count of each typical day is used as a frequency weight in the MILP objective function, ensuring that the annual energy cost calculation remains representative of full yearly operation. The resulting typical day profiles and their annual occurrence distribution are presented in Figures B.1 and B.2 in the Appendix, where the diversity across the 10 clusters confirms that the algorithm has successfully captured the principal seasonal and diurnal operating regimes of the system.

2.3. System integration and optimization framework

The integration of all subsystems is carried out using OSMOSE [18], an energy integration and optimization platform developed at EPFL. The mass and heat streams obtained from the Aspen Plus models are used as inputs to the system-level model, enabling the consistent representation of energy and material flows across all processes.

The overall system is formulated as a mixed-integer linear programming (MILP) problem as explained in [19,20]. The optimization determines the optimal sizing and operation of key system components, including electrolysis units, renewable generation capacities, CO_2 storage, and CO_2-to-ethanol conversion pathways. In particular, the operation and capacity of the CO_2 liquefaction and storage system are optimized to manage seasonal variations in CO_2 availability and renewable electricity supply.

The objective of the optimization is to evaluate system performance under variable renewable energy conditions, taking into account the electricity price variations. The framework enables the assessment of trade-offs between carbon utilization, energy efficiency, and economic performance, as well as the identification of optimal operational strategies for integrated PtL systems targeting SAF production.

3. Results and discussion

This section presents the results of the process modelling, heat integration analysis, CO_2 utilization pathway assessment, and seasonal storage optimization for the integrated biorefinery–PtL system.

3.1. Process heat integration

The grand composite curves (GCCs) of the two core processes, corn-to-ethanol production and ethanol-to-jet fuel (EtJ) upgrading, are presented in Figure 3. The GCC of the ethanol production process (Figure 3a) reveals a pinch point at 90°C with a minimum heating requirement of 98 MW (3.26 MWh/ton of ethanol production). This is considering the waste heat recovery from the separated vapor streams of DDGS production adapted from the reference model of [3]. The ethanol-to-jet (EtJ) process (Figure 3b) operates at significantly higher temperatures, with a pinch point at 350°C driven by the hydrotreating and dehydration reactions. The minimum heating requirement of 8.7 MW (0.29 MWh/ton of ethanol conversion) is significantly lower than the minimum cooling requirement of 23.9 MW (0.79 MWh/ton of ethanol conversion). The waste heat below the pinch temperature can be used to meet the heating demands of the corn-to-ethanol production process. This thermal complementarity between the two processes forms the thermodynamic basis for the integrated system configuration evaluated in this study. In addition, the off-stream from the recycling of the hydrotreating step in the EtJ process (consisting of 10% purge), along with the flue gas of the debutanizer distillation column, can be used for additional heat generation, which has also been evaluated.

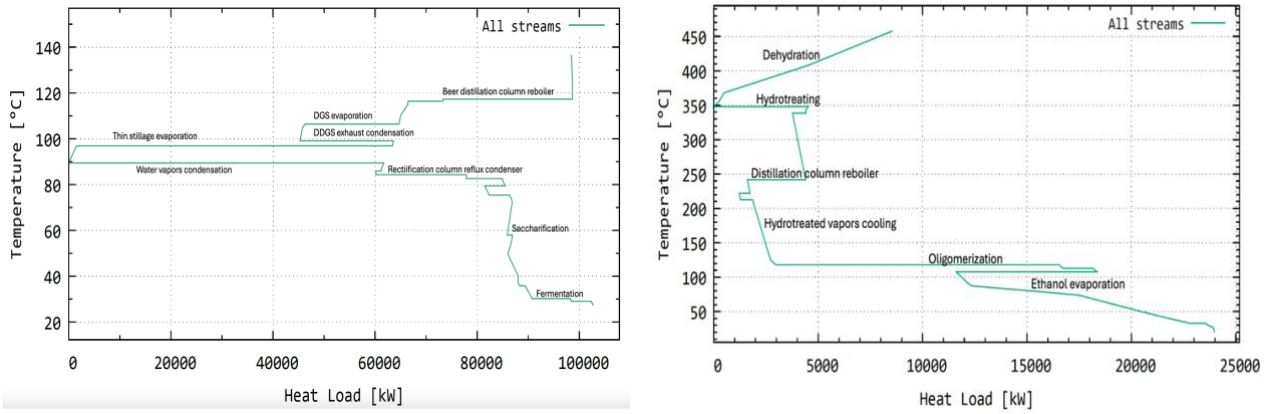

a) b)

Figure. 3. Grand composite curves of (a) the ethanol production process and (b) the ethanol-to-jet fuel (EtJ) process. The pinch point temperatures are 90 °C for (a) and 350 °C for (b), indicating potential for heat integration and waste heat recovery from the jet fuel process to the ethanol production process.

The grand composite curves of the two CO_2-to-ethanol conversion pathways are shown in Figure 4. The catalytic hydrogenation pathway (Figure 4a) is characterised by an exothermic heat profile dominated by purge gas combustion at temperatures up to ~1,000°C, which generates a large high-temperature heat surplus. The alkaline electrolyser appears as a low-grade heat sink near ambient temperature. Importantly, the heat released by purge gas combustion and hydrogenation reaction (at 200 °C) far exceeds the internal heat demand of the pathway, making the catalytic hydrogenation route a net heat-exporting process. This heat surplus is available for integration with the broader system, particularly the corn-to-ethanol production process. The syngas fermentation pathway via co-electrolysis (Figure 4b) presents a fundamentally different thermal profile. The Co-SOEC unit imposes a high-temperature heat demand peaking at 800°C. Unlike the catalytic hydrogenation route, this pathway is a net heat-consuming process requiring external thermal input to satisfy the co-electrolyser and distillation demands.

3.2. Process integration

The integrated composite curve of the full system incorporating the ethanol and jet fuel production process with biogenic CO_2 utilization via the catalytic hydrogenation pathway is shown in Figure 5. The curve reveals that the integrated system requires no external hot utility; the high-temperature heat released by purge and

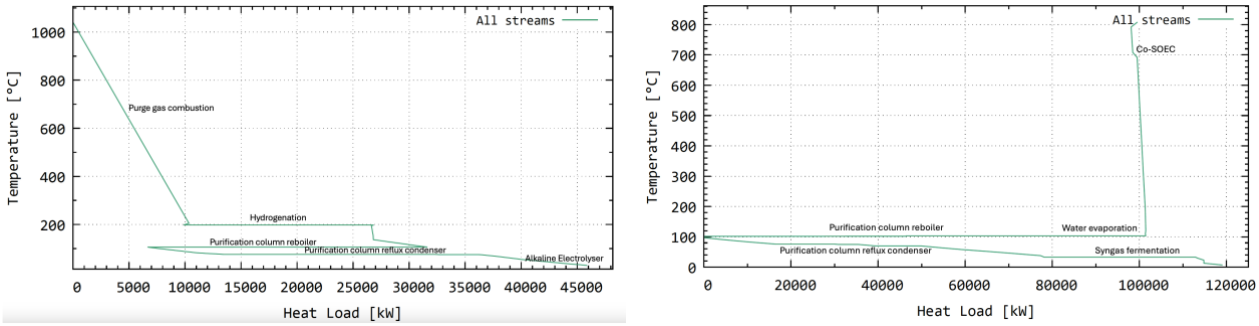

a) b)

Figure. 4. Grand composite curves of (a) catalytic hydrogenation and (b) syngas fermentation pathways for ethanol production from biogenic CO_2. Pathway (a) is exothermic, with purge gas enabling additional heat recovery. In contrast, pathway (b) is net heat demanding, due to the high-temperature requirement of the co-electrolyser (~800 °C) and the distillation process (~100 °C), while fermentation heat is released at low temperature (~35 °C), limiting its recovery potential.

flue gas combustion and exothermic reactions is sufficient to satisfy all internal heating demands. A cooling tower operating near ambient temperature constitutes the sole cold utility, absorbing the residual heat surplus that cannot be recovered internally. This thermally self-sufficient configuration demonstrates the strong synergistic potential of integrating the CO_2 utilization pathway with the jet fuel production process, as the exothermic character of the catalytic hydrogenation pathway contributes favourably to the overall heat balance. It is important to note that this result is specific to the CO_2 utilization case; the higher CO_2 discharge rate from the seasonal storage tank in this configuration drives an increased jet fuel production scale beyond what the individual pathway analysis in Figure 3(b).

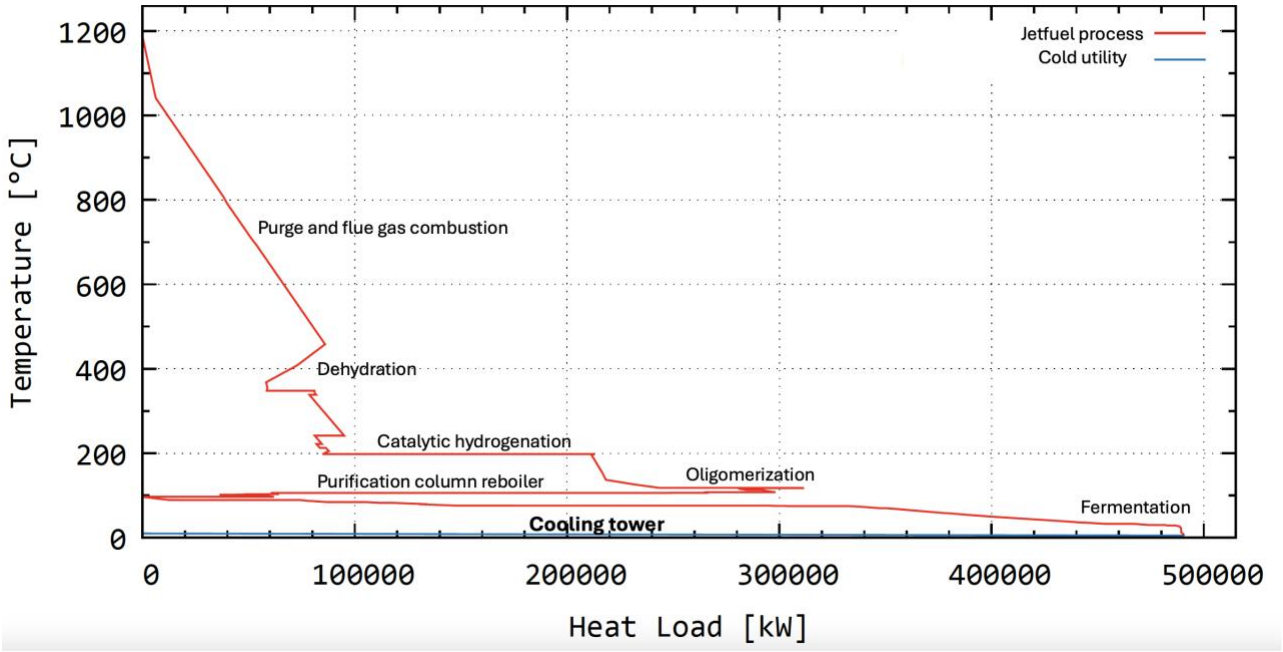

Figure. 5. Integrated composite curves of the jet fuel production process incorporating biogenic CO_2 utilization for additional fuel synthesis. The configuration requires no external hot utility and operates as a net heat-generating system.

3.3. CO_2 storage dynamics

The temporal variation of the CO_2 storage tank inventory over the full year is presented in Figure 6. The profile reveals a distinct seasonal pattern governed by the interplay between continuous CO_2 generation from the ethanol fermentation process and the variable utilization driven by renewable electricity availability and price dynamics.

During the winter and early spring months (January through April), CO_2 accumulates steadily in the storage tank, reaching a peak inventory of approximately 122k tonnes in April. This accumulation phase corresponds to a period of lower renewable electricity availability in Switzerland, particularly reduced solar irradiance, which limits the operation of the electrolysis-based CO_2 conversion pathway. The storage system, therefore, absorbs the mismatch between continuous CO_2 supply and intermittent conversion capacity, preventing CO_2 from being vented.

From May onwards, CO_2 inventory begins to decline as increasing solar generation and lower electricity prices enable higher utilisation rates. The drawdown accelerates through June and July, reflecting the summer peak in renewable electricity supply and the corresponding intensification of electrolyser and hydrogenation operation. The storage level approaches near-zero in September, indicating near-complete seasonal utilisation of the accumulated CO_2. From October onwards, the inventory begins to increase as declining renewable generation, and rising electricity prices reduce the economic incentive for CO_2 conversion. This behaviour confirms that the CO_2 storage system fulfils its intended role as a seasonal energy storage buffer, decoupling CO_2 availability from conversion capacity and enabling the system to exploit renewable electricity at times of greatest economic and environmental benefit.

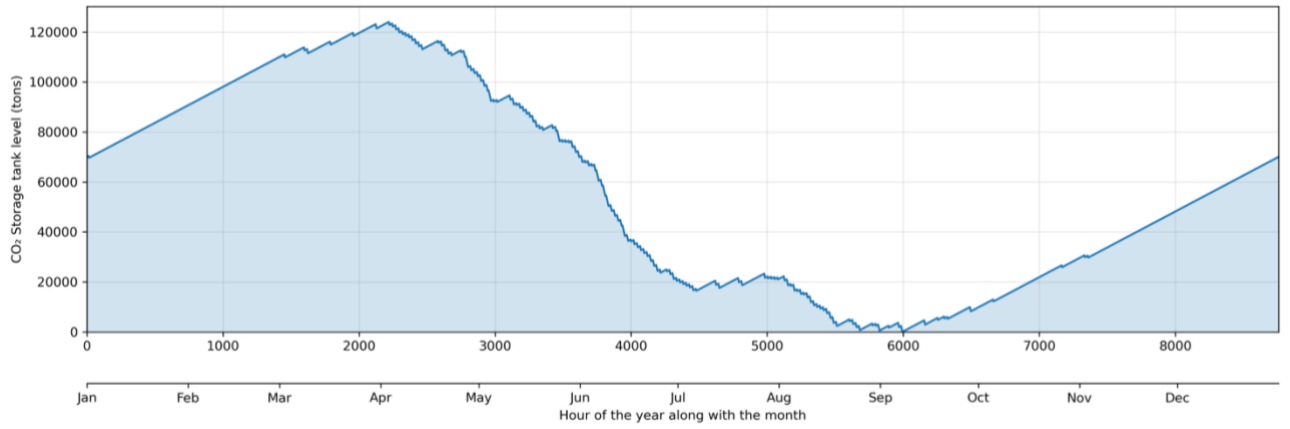

Figure. 6. Temporal variation of CO_2 inventory in the storage tank, showing accumulation during periods of high electricity price and utilization during low-price periods, highlighting its role as seasonal energy storage.

4. Conclusion

This study presented an integrated biorefinery–PtL framework for biogenic CO_2 utilization in SAF production, evaluated through process integration and MILP-based optimization under variable renewable energy conditions.

The heat integration analysis demonstrated strong thermal complementarity between the corn-to-ethanol and ethanol-to-jet fuel processes, with the high-grade waste heat available from the jet fuel upgrading section capable of satisfying the heating demands of the ethanol production process. Among the two CO_2 utilization pathways evaluated, the catalytic hydrogenation route exhibited a net heat-exporting character driven by purge gas combustion, in contrast to the syngas fermentation pathway, which imposes a significant external heat

demand due to the high-temperature co-electrolyser requirement and ethanol purification, while fermentation heat is released at a temperature of ~35°C.

When the catalytic hydrogenation pathway, along with CO_2 storage, is integrated with the full system, the configuration achieves complete thermal self-sufficiency with no external hot utility requirement. This configuration also benefits from the higher CO_2 discharge rate enabled by seasonal storage, which drives an increased jet fuel production scale relative to standalone pathway operation, significantly improving the overall energy efficiency and economic attractiveness of the integrated biorefinery.

The seasonal CO_2 storage analysis confirmed that liquefaction-based storage effectively decouples CO_2 supply from renewable electricity availability, enabling near-complete annual utilization of the biogenic CO_2 stream by exploiting periods of high renewable generation and low electricity prices.

Future work will focus on the valorisation of DDGS as an additional feedstock for further fuel production within the biorefinery framework.

References

[1] Uddin, Md Mosleh et al. (Nov. 2025). “Sustainable aviation fuel from ethanol: Techno-economic analysis and life cycle analysis”. In: Applied Energy 398, p. 126373. ISSN: 0306-2619. DOI: 10.1016/j.apenergy.2025.126373

[2] Zhang, Xin et al. (July 2025). “Comprehensive design and scheduling optimization of a photovoltaic-wind-solid waste hybrid power system for green hydrogen and methanol production”. In: International Journal of Hydrogen Energy 152, p. 149892. ISSN: 0360-3199.

[3] Kwiatkowski, Jason R. et al. (May 2006). “Modeling the process and costs of fuel ethanol production by the corn dry-grind process”. In: Industrial Crops and Products 23.3, pp. 288–296. ISSN: 0926-6690

[4] Tao, Ling et al. (2017). “Techno-economic analysis for upgrading the biomass-derived ethanol-to-jet blendstocks”. In: Green Chem. 19.4, pp. 1082–1101. DOI: 10.1039/C6GC02800D.

[5] He, Xinyi (Nov. 2017). “CO2 Hydrogenation for Ethanol Production: A Thermodynamic Analysis”. In: International Journal of Oil, Gas and Coal Engineering 5, p. 145.

[6] Ding, Liping et al. (Oct. 2020). “CO2 Hydrogenation to Ethanol over Cu@Na-Beta”. In: Chem 6.10, pp. 2673–2689. ISSN: 2451-9294

[7] He, Yiming et al. (July 2023). “Assessing the efficiency of CO2 hydrogenation for emission reduction: Simulating ethanol synthesis process as a case study”. In: Chemical Engineering Research and Design 195, pp. 106–115. ISSN: 0263-8762.

[8] He, Yiming et al. (Feb. 2024). “Thermodynamic analysis of ethanol synthesis by CO2 hydrogenation using Aspen Plus: effects of tail gas recycling and CO co-feeding”. In: Chemical Engineering Communications 211.2. _eprint: https://doi.org/10.1080/00986445.2023.2240709, pp. 300–310. ISSN: 0098-6445.

[9] Liew, FungMin et al. (May 2016). “Gas Fermentation—A Flexible Platform for Commercial Scale Production of Low-Carbon-Fuels and Chemicals from Waste and Renewable Feedstocks”. English. In: Frontiers in Microbiology 7. ISSN: 1664-302X.

[10] Regis, Francesco, Alessandro Hugo Antonio Monteverde and Debora Fino (July 2023). “A techno-economic assessment of bioethanol production from switchgrass through biomass gasification and syngas fermentation”. In: Energy 274, p. 127318. ISSN: 0360-5442

[11] Lee, Uisung et al. (2021). “Using waste CO2 from corn ethanol biorefineries for additional ethanol production: life-cycle analysis”. en. In: Biofuels, Bioproducts and Biorefining 15.2. _eprint: https://scijournals.onlinelibrary.wiley.com/doi/pdf/10.1002/bbb.2175, pp. 468–480. ISSN: 1932-1031.

[12] Huang, Zhe et al. (Dec. 2020). “Using waste CO2 to increase ethanol production from corn ethanol biorefineries: Techno-economic analysis”. In: Applied Energy 280, p. 115964. ISSN: 0306-2619.

[13] Domingos, Meire Ellen Gorete Ribeiro et al. (Aug. 2023). “Multi-time integration approach for combined pulp and ammonia production and seasonal CO2 management”. In: Computers & Chem-

ical Engineering 176, p. 108305. ISSN: 0098-1354.
[14] Flórez-Orrego, Daniel et al. (July 2025). “Integration of renewable energy and reversible solid oxide cells to decarbonize secondary aluminium production and urban systems”. en-CA. In: Systems and Control Transactions, pp. 546–552.
[15] ENTSO-E. URL : https://www.entsoe.eu/
[16] Ashouri, Araz et al. (Sept. 2013). “Optimal design and operation of building services using mixed-integer linear programming techniques”. In: Energy 59, pp. 365–376. ISSN: 0360-5442.
[17] Wang, Yun et al. (Dec. 2019). “Approaches to wind power curve modeling: A review and discussion”. In: Renewable and Sustainable Energy Reviews 116, p. 109422. ISSN: 1364-0321
[18] Dardor, Dareen et al. (Sept. 2024). “ROSMOSE: A web-based decision support tool for the design and optimization of industrial and urban energy systems”. In: Energy 304, p. 132182. ISSN: 0360-5442.
[19] Flórez-Orrego, Daniel, Meire Domingos and François Maréchal (Sept. 2022). A systematic framework for the multi-time integration of industrial complexes and urban systems. CPOTE 2022, Warsaw, Poland
[20] Baibhav, Vibhu et al. (July 2025). Process integration and waste valorization for sustainable biodiesel production toward a transportation sector energy transition. Pages: 875. DOI:10.69997/sct. 147707.

Appendix A: PV and wind power generation models

This section presents the mathematical models used to characterize the power output of the photovoltaic (PV) array and the wind turbine installation. Both technologies are incorporated into the MILP optimization framework as scalable power generation assets. The PV system is subject to a maximum installable panel area constraint of A_{PV}, while the wind installation is bounded by a maximum number of turbine units N_{WT}.

A.1 Photovoltaic generation model

The PV output model accounts for the temperature-dependent degradation of panel efficiency under real operating conditions. The model estimates the actual panel temperature from ambient conditions and solar irradiance, and corrects the efficiency accordingly. The operating temperature of the PV panel, T_{panel}, is derived from a thermal equilibrium between heat gain from solar irradiance and heat loss through the glazing layer. It is expressed as:

$$T_{panel} = \frac{U_{glass}(T_{ext} + 273.15)}{U_{glass} - \eta_{var} \cdot GI} + \frac{GI\left(f_{glass} - \eta_{ref} - \eta_{var} T_{ref}\right)}{U_{glass} - \eta_{var} \cdot GI}$$

where T_{ext} is the external ambient temperature (°C), GI is the incident solar irradiance (W/m²), U_{glass} = 29.1 W/m²K is the overall heat loss coefficient of the glazing layer accounting for both convective and radiative losses, f_{glass} = 0.9 is the fraction of irradiance absorbed by the panel, η_{ref} = 0.14 is the panel's nominal electrical efficiency at reference conditions, and T_{ref} = 298 K is the reference temperature. The parameter η_{var} = 0.001 /K is the temperature coefficient of efficiency and captures the sensitivity of electrical output to thermal deviation. The effective PV efficiency, η_{PV} at operating conditions is then computed as:

$$\eta_{PV} = \eta_{ref} - \eta_{var}\left(T_{panel} - T_{ref}\right)$$

The electrical energy generated by the PV array over a given time step is:

$$E_{PV} = GI \cdot A_{PV} \cdot \eta_{PV}$$

where A_{PV} is the installed panel area (m²), bounded in the optimization problem by the site constraint.

A.2 Wind power generation model

The wind power model translates measured near-surface wind speed data into turbine electrical output, accounting for hub height correction, air density variation with temperature, rotor geometry, and a piecewise turbine power curve.

Atmospheric air density varies with temperature and directly affects the kinetic energy content of the wind. It is estimated using the ideal gas approximation:

$$\rho_{air} = 1.293 \cdot \frac{273.15}{T_{ext} + 273.15}$$

where 1.293 kg/m³ is the air density at 0°C and standard pressure, and the ratio corrects for the actual ambient temperature T_{ext} in degrees Celsius. Wind speed measurements are typically recorded at a standard meteorological height of z_{mea} = 10 m. To obtain the wind speed at rotor hub height, a power-law wind shear profile is applied:

$$V_{real} = V_{mea}\left(\frac{z_{rotor}}{z_{mea}}\right)^{\alpha}$$

where V_{mea} is the measured wind speed at reference height, Z_{rotor} = 71.5 m is the hub height, and α = 0.25 is the wind shear exponent. The rotor swept area is calculated from the turbine rotor diameter d_{rotor} = 82 m:

$$A_{rotor} = \frac{\pi d_{rotor}^2}{4}$$

The actual electrical output of the wind turbine installation incorporates the aerodynamic power coefficient C_p, mechanical drivetrain efficiency η_{mech}, and a piecewise operating envelope defined by the turbine's cut-in, rated, and cut-out wind speeds:

$$P_{WT} = \begin{cases} 0, & V < 3 \text{ or } V > 25 \\ \frac{1}{2} N_{WT} \rho_{air} A_{rotor} \eta_{mech}\, c_p\, V^3 & ,3 \le V \le 12 \\ \frac{1}{2} N_{WT} \rho_{air} A_{rotor} \eta_{mech}\, c_p\, 12^3\,, & 12 < V \le 25 \end{cases}$$

where N_{WT} is the number of installed wind turbines, C_p = 0.49 is the power coefficient of the rotor blades, and η_{mech} = 0.90 accounts for mechanical losses in the drivetrain between the rotor shaft and the generator. The three operating regions are defined as follows: below the cut-in speed of 3 m/s, insufficient torque is generated and output is zero; between 3 and 12 m/s, output follows the cubic wind speed relationship scaled by rotor and loss parameters; above the rated speed of 12 m/s and up to the cut-out speed of 25 m/s, output is capped at the rated power corresponding to V = 12 m/s to protect the turbine from mechanical overload. Beyond 25 m/s, the turbine is shut down and output returns to zero.

Appendix B: Typical day clustering results

The following figures present the K-means clustering results derived from the 8,760-hour annual dataset.

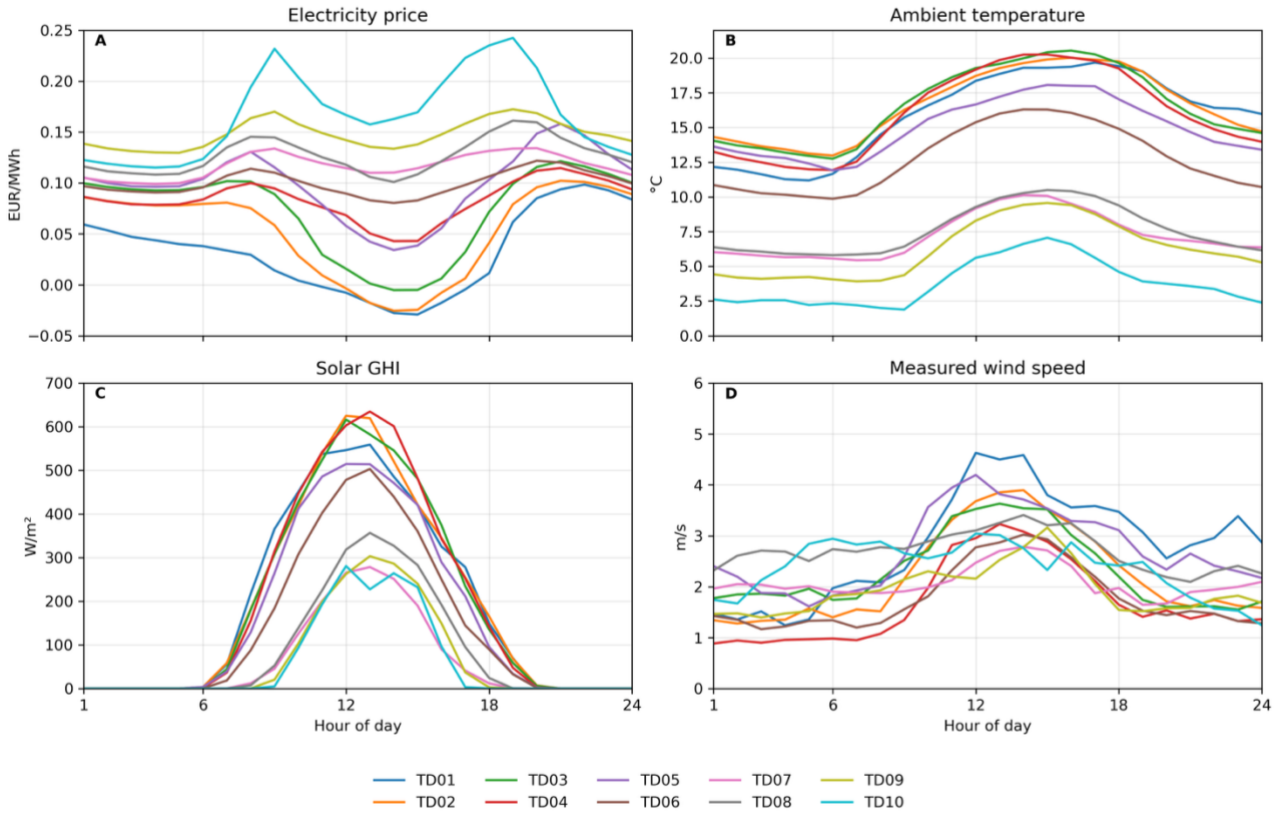

Figure. B.1. Hourly profiles of electricity price, ambient temperature, global solar irradiance, and wind speed for the 10 typical days identified through K-means clustering of the 8,760-hour annual dataset.

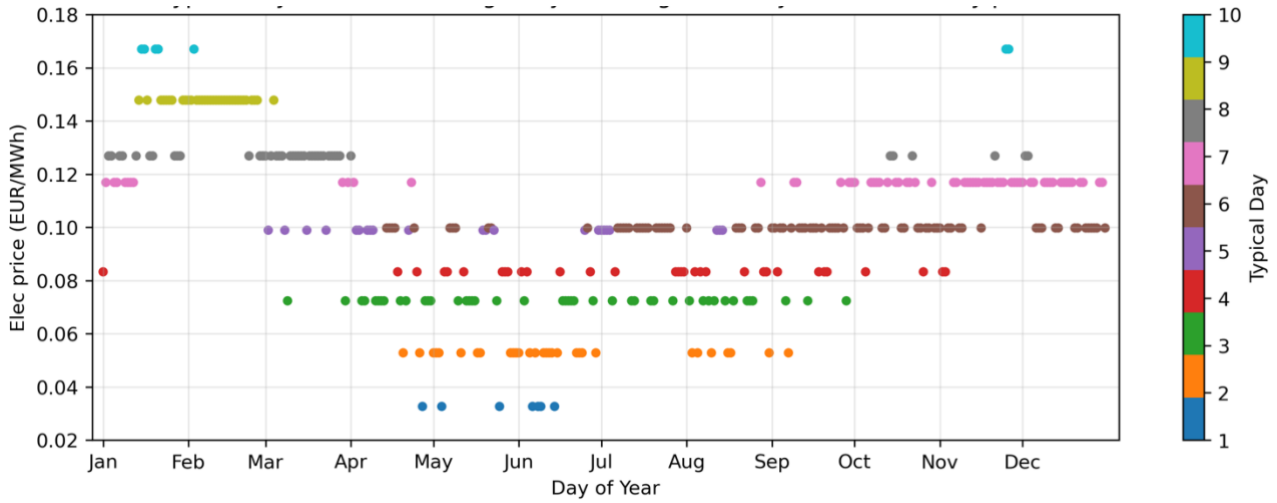

Figure. B.2. Typical day occurrences during the year, along with the daily mean electricity price.